Long-term monthly statistics of the mid-latitude ionospheric E-layer peak electron density in the Northern geographic hemisphere during geomagnetically quiet and steadily low solar activity conditions

Anatoli V. Pavlov [1,★], Nadezhda M. Pavlova[1]

[1] Pushkov Institute of Terrestrial Magnetism, Ionosphere and Radio-Wave Propagation of the Russian Academy of Sciences (IZMIRAN), Moscow, Troitsk, Russia

ABSTRACT

Long-term hourly values of the ionospheric E-layer peak electron density, NmE, measured from 1957 to 2014 by 4 mid-latitude ionosondes (Wallops Island, Boulder, de l'Ebre, and Rome) in the Northern geographic hemisphere were processed to select periods of geomagnetically quiet and low solar activity conditions using the 3-hour index, Ap, of geomagnetic activity and the daily solar 10.7 cm radio flux index, F10.7, of solar activity. The selected ionospheric E-layer peak electron densities are used to calculate several descriptive statistics of NmE close to noon for each month in a year, including the mathematical expectation of NmE, the standard deviation of NmE from the mathematically expected NmE, and the coefficient of variations of NmE. The month-to-month variability of these descriptors allowed us to identify months when they reach their extremes (maxima, minima).

1. Introduction

Production and loss processes of ions and electrons of the mid-latitude ionospheric E-region are well studied [see, e.g., *Schunk and Nagy*, 2009; *Pavlov*, 2012, *Pavlov and Pavlova*, 2013, 2015, and references therein]. Analyzing production and loss rates of ions and electrons of the ionospheric E-region, it is possible to establish causes of day-to-day variations of the mid-latitude E-region peak electron density, NmE, during each month of a year under given local time, latitude, and longitude. The major sources of this variability of NmE are changes of X-ray and EUV solar irradiance with solar activity, variations of number densities and temperature of neutral species with solar and geomagnetic activity, and changes of the solar zenith angle [e.g., *Moore et al.*, 2006, *Pavlov and Pavlova*, 2013, 2015].

Day-to-day variability of ionospheric E-region electron densities remains a topic of interest [see, e.g., *Kouris and Fotiadis*, 2002; *Moore et al.*, 2006; Ni-colls et al., 2012, and references therein]. The hourly values of the critical frequency, foE (which is proportional to the square root of NmE [*Piggot and Raver*, 1978]), of the ionospheric E-layer measured by 30 mid-latitude ionosondes during the period of 1964-1995 were used by *Kouris and Fotiadis* [2002] to evaluate day-to-day variability of foE. They found that positive and negative relative deviations of foE from the monthly median values of foE are within the range of 10 % for more than 90 % of the time. Noontime day-to-day ionosonde and incoherent scatter radar measurements of the E layer parameters were used by *Moore et al.* [2006] to calculate the standard relative deviations of NmE from noontime NmE mean values in the range of 5-7% at middle latitudes for 9–27 March 1999 and 4 October – 4 November 2002. Slightly larger values of NmE variability were estimated by *Nicolls et al.* [2012] using the inversion technique from satellite-based radio occultation total electron content measurements. However, little attention has been given in these and other published morphological studies to NmE data sorting due to apparent variability of solar and geomagnetic activity. Thus, this published NmE statistics in fact describes a mix of day-to-day variations of geomagnetically quiet NmE at a steady solar activity and variations of NmE in response to changing geomagnetic and solar activity conditions.

The daily solar 10.7 cm radio flux index, F10.7, (or a daily sunspot number) and the 3-hour geomagnetic index, Ap (or Kp), are the most widely used indices for exploring causes and consequences of solar and geomagnetic activity [see, e.g., *Akasofu and Chapman*, 1972; *Schunk and Nagy*, 2009]. Therefore, the F10.7 and

Ap indices are used in our work to describe dependencies of NmE on solar and geomagnetic activities, respectively.

NO^+ and O_2^+ ions are the main ions at the E-region altitudes of the ionosphere, and the characteristic time to approach the photochemical equilibrium by dissociative recombination reactions of these ions with electrons is less than one minute during daytime conditions close to the E-layer peak altitude [*Banks and Kockarts*, 1973]. The value of this characteristic time is much less than 3 hours. As a result, variations of NmE caused by changes in geomagnetic activity during a period that is less than 3 hours are not described in terms of changes of Ap and can be considered as random variations of NmE if the Ap index is used to study a dependence of NmE on geomagnetic activity.

The sun is not static throughout each day, and changing X-ray and EUV irradiance with time periods less than 24 hours are not captured by the F10.7 index of solar activity or by any other daily index of solar activity [*Acebal and Sojka*, 2011]. Hence, if the solar ionizing fluxes are changing significantly during a few hours due to flares and also an overall background change, the daytime NmE will respond, but this response of NmE cannot be described in terms of variations of F10.7. It should be also noted that the integral solar flux below 200 nm increases with a rise in the average index $0.5(F10.7+\overline{F10.7})$ only on average, and there are significant deviations from the linear correlation between this integral solar flux and this average index where $\overline{F10.7}$ is the 81-day average of daily F10.7 solar activity indices centered on the day under study [*Solomon*, 2006]. *Manson* [1976] has also pointed out that the correlation of the integrated solar flux between 5.2 nm and 12 nm with F10.7 is poor.

On the other hand, there is significant influence of variations in X-ray irradiance on NmE [*Pavlov and Pavlova*, 2013, 2015, *Sojka et al.*, 2014]. From the above reasoning, differences between NmE calculated by the one-dimensional time-dependent theoretical mid-latitude model of the E-region ion composition and NmE measured by the Boulder and Moscow ionosondes can be explained by uncertainties up to a factor of 2 in predictions of X-ray radiation on the basis of changes in the F10.7 and $\overline{F10.7}$ indices [*Pavlov and Pavlova*, 2013, 2015]. As a result, the use of the F10.7 index as an indicator of solar activity in statistical studies of NmE can be one of sources of deviations of NmE from the expected NmE for the chosen level of solar activity, and these deviations caused by the use of the F10.7 index can be considered as random variations of NmE.

The quiet time ionospheric E-layer number densities measured by an ionosonde during a month depend on the solar zenith angle which value is changed during this month. However, the existence of a day in a month at low solar activity does not mean that all days in this month correspond to the low solar activity conditions under consideration. In addition to that, geomagnetically quiet time periods are randomly distributed during each month of a year. Thus, day-to-day variability of NmE at given local time during each month of a year caused by changes of the solar zenith angle is modified in a random way due to variations of solar and geomagnetic activity.

The foregoing shows that the daytime value of NmE measured by an ionosonde during geomagnetically quiet conditions at low solar activity under given local time during a month in a year can be considered as a random variable. The objective of this work is to apply the mathematical statistics, as described, for example, by *Johnson and Leone* [1977], to study this variability of NmE using NmE measured by the mid-latitude ionosondes at Wallops Island, Boulder, de l'Ebre, and Rome in the Northern geographic hemisphere from 1957 to 2014 during geomagnetically quiet conditions at low solar activity. For achievement of this purpose, we calculate the mathematically expected, <NmE>, and most probable, NmE_{MP}, values of NmE, the standard deviations of NmE from <NmE> and NmE_{MP}, and the coefficients of variations of NmE relative to <NmE> and NmE_{MP} for each month of a year using data collected by 4 mid-latitude ionosondes in the Northern geographic hemisphere. As a result, month-to-month variations of the above listed statistical parameters of NmE over each ionosonde are studied.

2. Data and Method of Data Analysis

The ionosonde data for this investigation were obtained from the NOAA National Geophysical Data Center (NGDC) in Boulder, Colorado, using its online Space Physics Interactive Data Resource (SPIDR). First, we selected the hourly values of foE observed in 1957-2014 by 4 ionosondes (Wallops Island, Boulder, de l'Ebre, and Rome) in the Northern geographic hemisphere. Table 1 provides the geographic latitude and longitude (ϕ, λ), and average geomagnetic latitude and longitude (Φ, Λ) of each ionosonde. The ionosonde stations presented in Table 1 are listed in order of increasing geographic latitude. It follows from the calculations [details are described by *Pavlov and Pavlova*, 2014] that the geomagnetic coordinates of the ionosondes under consideration averaged over the time

period from 1957 to 2012 and given by *Pavlov and Pavlova* [2014] are practically the same as for the time period of 1957-2014, and these average values of Φ and Λ are presented in Table 1. We believe that, under quiet geomagnetic conditions, the mid-latitude ionosphere is located between 30° and 55° geomagnetic latitudes in the Northern geographic hemisphere. The stations used are all located within the 30° to 55° geomagnetic latitude interval, representing the mid-latitude ionosphere.

NmE values were obtained from foE using their well known relationship [e.g., *Piggott and Rawer*, 1978]

$$NmE = 1.24 \cdot 10^4 \, foE^2, \tag{1}$$

where the units of NmE and foE are cm^{-3} and MHz, respectively.

The hourly foE records acquired from the NGDC archives were analyzed to select values corresponding to time points during the geomagnetically quiet periods defined below with UT closest to the solar noon in the solar local time, SLT (see Table 1). The relationship between UT and SLT is defined by UT=SLT-λ/15, where λ is the East geographic longitude of the ionospheric observatory in degrees, while SLT and UT come in units of hours. It should be noted that the values of foE measured by the Juliusruh ionosonde at 10:58 UT are provided by the NGDC archives for the time period from 26 March 2007 to 31 December 2014, and these measurements are used in our statistical study in place of missing Juliusruh ionosonde measurements of foE at 11:00 UT for this time period (see Table 1).

The E-region ion and electron densities depend on geomagnetic activity due to variations of the neutral temperature and densities with geomagnetic activity. These changes in the neutral temperature and densities can be described by variations of 7 indices: the daily Ap index, the 3-hour Ap index for current time, the 3-hour Ap indices for 3, 6, and 9 hours before current time, the average of eight 3-hour Ap indices from 12 to 33 hours prior to current time, and the average of eight 3-hour Ap indices from 36 to 57 hours prior to current time [*Hedin*, 1987; *Picone et al.*, 2002]. The relationship between indices Ap and Kp is well established, and the value of Ap=18 corresponds to Kp=3 [*Akasofu and Chapman*, 1972]. The geomagnetically quiet conditions for the candidate noon foE values were identified by ensuring that each of the seven above-mentioned indices of geomagnetic activity was equal to 18 or was less than 18. To select periods of steadily low solar activity, we relied on analysis of three indices derived from observations of F10.7. The solar EUV flux, primarily responsible for the daytime ionization, is approximately represented by F10.7 and $\overline{F10.7}$ [*Richards et al.*, 1994]. The electron density also depends on the solar-controlled neutral temperature and densities whose dependences on F10.7p (F10.7 for a day preceding a day under consideration) and $\overline{F10.7}$ are well established [*Hedin*, 1987; *Picone et al.*, 2002]. All three indices, F10.7, F10.7p, and $\overline{F10.7}$, were used to control selection of the *fo*E data by retaining only those days for which these indices were within the 65 to 85 interval (in 10^{-22} W·m^{-2}·Hz^{-1}).

We consider sets of foE(UT,M) and NmE(UT,M) for each month, M, in a year at the given UT for each location. The results of measurements of foE are presented in the database with the step, ΔfoE, of 0.05 MHz, i.e. the considered foE are given on the

Ionosonde	φ (°)	λ (°)	Φ (°)	Λ (°)	Years	UT	SLT
Wallops Island	37.8	284.5	45.3	358.6	1967-2014	17:00	11:58
Boulder	40.0	254.7	46.9	325.2	1958-1960, 1962-2002, 2004-2014	19:00	11:59
De l'Ebre	40.8	0.3	40.8	76.7	1957-1980, 1982-1987, 1991-1995, 1998-2004, 2007-2014	12:00	12:01
Rome	41.8	12.5	40.0	88.4	1976-2004, 2007-2014	11:00	11:50

Table 1. The ionosonde names and locations, and time ranges of foE measurements at the universal time, UT, closest to the solar noon in the solar local time, SLT.

uniform grid of $foE_k = k\Delta foE$, where $k = 1, 2, \ldots K$, and K is the maximal value of k. The measured critical frequencies foE_k and Eq. (1) allow to determine the corresponding measured E-layer peak electron densities NmE_k at the corresponding non-uniform grid of NmE_k.

The probability, $P_k(UT,M)$, to measure a geomagnetically quiet $NmE_k(UT,M)$ is counted individually for each ionosonde, UT, and M as

$$P_k(UT,M) = F_k(UT,M)/F(UT,M), \quad (2)$$

where $F_k(UT,M)$ is a number of $NmE_k(UT,M)$, $F(UT,M) = \sum_{k=1}^{K} F_k(UT,M)$ is the total number of selected $NmE_k(UT,M)$ values.

It follows from Eq. (2) that $\sum_{k=1}^{K} P_k(UT,M) = 1$.

It should be noted that the value of $F(UT,M)$ turned out to be at least 101 or greater than 101 for each ionosonde. We believe that this value of $F(UT,M)$ is enough large to carry out our statistical study.

We define the mathematical expectation of NmE to be

$$<NmE(UT,M)> = \sum_{k=1}^{K} P_k(UT,M) NmE_k \quad (3)$$

The standard deviation of NmE from <NmE> is calculated as

$$\sigma_{AV}(UT,M) = \{\sum_{k=1}^{K} P_k(UT,M)[NmE_k - <NmE(UT,M)>]^2\}^{0.5}. \quad (4)$$

The coefficient of variations of NmE relative to <NmE> (the relative standard deviation of NmE from <NmE>) expressed as a percentage takes a form

$$CV_{AV}(UT,M) = 100\sigma_{AV}(UT,M)/<NmE(UT,M)>. \quad (5)$$

All values of NmE_k are not equally probable, and P_k reaches its maximum at the most probable value, NmE_{MP}, of NmE. The standard deviation, σ_{MP}, of NmE from NmE_{MP} and the coefficient, CV_{MP}, of variations of NmE relative to NmE_{MP} (the relative standard deviation of NmE from NmE_{MP}) are calculated as

$$\sigma_{MP}(UT,M) = [\sum_{k=1}^{K} P_k(UT,M)(NmE_k - NmE_{MP})^2]^{0.5}. \quad (6)$$

$$CV_{MP}(UT,M) = 100\sigma_{MP}(UT,M)/NmE_{MP}. \quad (7)$$

3. Results and Discussion

The use of the statistical approach to study month-to-month variations in the statistical parameters of NmE is motivated by a variability of NmE during geomagnetically quiet conditions for approximately the same solar activity at the same UT and location during each month. If these conditions are carried out then day-to-day variability of NmE determines a dependence of $P_k(UT,M)$ on NmE_k. Examples of this dependence are shown in Figure 1 when the Boulder ionosonde data at 19:00 UT (11:59 SLT) are used in the statistical study. Circles and pluses in Figure 1 correspond to January and February (left top panel), March and April (left middle panel), May and June (left bottom panel), July and August (right top panel), September and October (right middle panel), and November and December (right bottom panel), respectively.

It follows from the calculations that each dependence of $P_k(UT,M)$ on NmE_k (see Figure 1) is a sequence of peaks in $P_k(UT,M)$, and a location of the largest peak in the NmE_k–axes determines the most probable, NmE_{MP}, value of NmE for each month under consideration. Figure 1 shows that, with the exception of the March dependence of $P_k(UT,M)$ on NmE_k, each of the dependences of $P_k(UT,M)$ on NmE_k has a peak in $P_k(UT,M)$ whose amplitude is not much less than that of the largest peak in $P_k(UT,M)$ for this dependence. It should be noted that the mathematical expectation of NmE defined by Eq. (3) takes into account the relative contribution of each value of NmE_k in accordance with the value of $P_k(UT,M)$ for this NmE_k, and all significant peaks in each dependence of $P_k(UT,M)$ on NmE_k under consideration are taking into account in <NmE>.

Figures 2-4 show month-to-month variations in the calculated values of <NmE> (crosses in Figure 2), NmE_{MP} (squares in Figure 2), σ_{AV} (crosses in Figure 3), σ_{MP} (squares in Figure 3), CV_{MP} (crosses in Figure 4), and CV_{MP} (squares in Figure 4) over the Wallops Island (left top panels), Boulder (left bottom panels), de l'Ebre (right top panels), and Rome (right bottom panels) ionosondes. It follows from our calculations that each statistical parameter of NmE is changed from ionosonde to ionosonde for the same month due to differences in geographic latitudes and longitudes of the ionosondes and in the values of SLT when these measurements were carried out by the ionosondes (see Table 1).

Percent differences between NmE_{MP} and <NmE> can be calculated for each month in a year as $200|NmE_{MP} - <NmE>|/(NmE_{MP} + <NmE>)$. This difference depends on M, and reaches its maximum value, $Z(NmE_{MP}, <NmE>)$, that varies from an ionosonde to an ionosonde. We found that $Z(NmE_{MP}, <NmE>) = 8.1, 6.1, 4.4,$ and 4.5 % for the Wallops Island, Boulder, de l'Ebre, and Rome ionosondes, respectively.
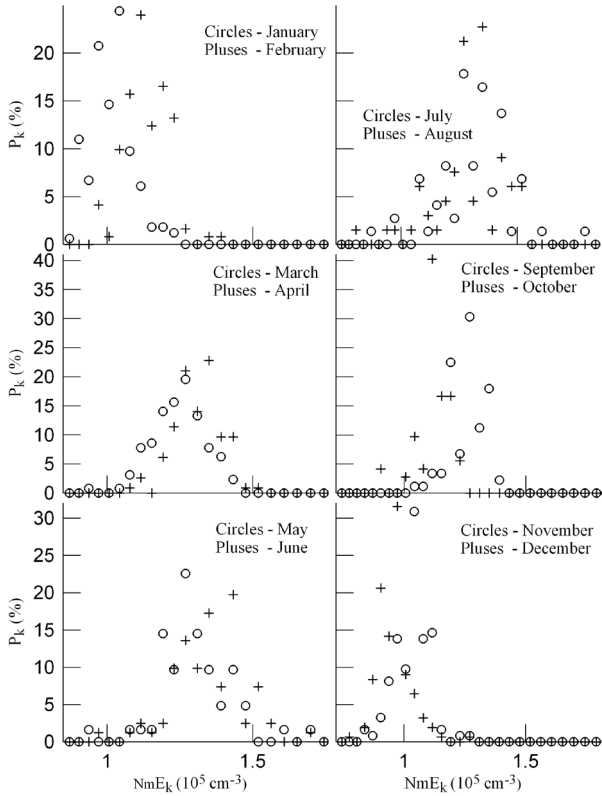
The calculated month-to-month variations of

Figure 1. Dependencies of $P_k(UT,M)$ on NmE_k over the Boulder ionosonde. Circles and pluses correspond to January and February (left top panel), March and April (left middle panel), May and June (left bottom panel), July and August (right top panel), September and October (right middle panel), and November and December (right bottom panel).

$<NmE>$ and NmE_{MP} shown in Figure 2 are both trying to estimate month-to-month variations of NmE. What is better?

It follows from the calculations of σ_{AV} and σ_{MP} presented in Figure 3 that

$$\sigma_{AV}(UT,M) < \sigma_{MP}(UT,M) \qquad (8)$$

The standard deviations of NmE from $<NmE>$ and NmE_{MP} measure spreads of distributions of NmE about $<NmE>$ and NmE_{MP}, respectively. We believe that, the smaller this spread, the more efficient the estimation. As a result, the calculated month-to-month variations of $<NmE>$ presented in Figure 2 can be considered as the most efficient estimation of month-to-month variations of NmE for the ionosonde measurements under consideration.

The calculations show (see Figure 4) that, as a rule, $CV_{AV}(UT,M) < CV_{MP}(UT,M)$ with the exception of M=2, 6, 7, 10, and 11 for the Rome, Delebre, Rome, Wallops Island, and Delebre ionosonde, respectively, and a difference between $CV_{AV}(UT,M)$ and $CV_{MP}(UT,M)$ is negligible for each of these exceptions. Thus, the calculated month-to-month variations of

$<NmE>$ can be considered as the most efficient estimation of month-to-month variations of NmE if we compare not only $\sigma_{AV}(UT,M)$ with $\sigma_{MP}(UT,M)$ but also $CV_{AV}(UT,M)$ with $CV_{MP}(UT,M)$. Based on this conclusion, the calculated month-to-month variations of NmE_{MP}, σ_{MP}, and CV_{MP} are not discussed further.

It follows from Figure 2 that the annual maximum of $<NmE>$ is formed in May (Wallops Island and Rome), June (Boulder), and July (de l'Ebre). The mathematical expectation of NmE is lowest in its annual value in December. A ratio of the largest to lowest value of the mathematically expected NmE characterizes the maximal month-to-month variability of this statistical parameter of NmE in a year. This ratio is found to be 1.40, 1.41, 1.43, and 1.43 for the Wallops Island, Boulder, de l'Ebre, and Rome ionosondes. We also point out that local minima of $<NmE>$ are formed in May, June, and July over the Boulder, Rome, and Wallops Island ionosondes, respectively.

By analogy with the definition of the winter anomaly of the F2-layer peak electron density (see, e.g., *Pavlov and Pavlova* [2005, 2009], *Pavlov et al.* [2010], and references therein), the winter anomaly of NmE can be defined as follows. If the E-layer peak electron density is sometimes greater in winter than that in summer over the same Earth's surface point during geomagnetically quiet daytime conditions at the same universal time despite the reduced solar insolation in winter in comparison with that in summer then this ionospheric phenomenon can be designated as the winter anomaly of NmE. It follows from Figure 2 that the winter anomaly of $<NmE>$ is not observed over the Wallops Island, Boulder, de l'Ebre, and Rome ionosondes.

It is seen from Figure 3 that the annual maximum of the standard deviation of NmE from $<NmE>$ occurs in July over all ionosondes under consideration. The lowest annual value of σ_{AV} is found to be in January (de l'Ebre), February (Wallops Island), October (Boulder), and December (Rome).

Figure 4 shows that the coefficient of variations of NmE maximizes in its annual value in July. This coefficient minimizes in its annual value in January (de l'Ebre), February (Wallops Island), September (Boulder), and October (Rome). It follows from the comparison of CV_{AV} of all 4 ionosondes that CV_{AV} reaches its lowest and largest values in its month-to-month variations over the de l'Ebre and Wallops Island ionosondes, respectively. If all 4 ionoson-
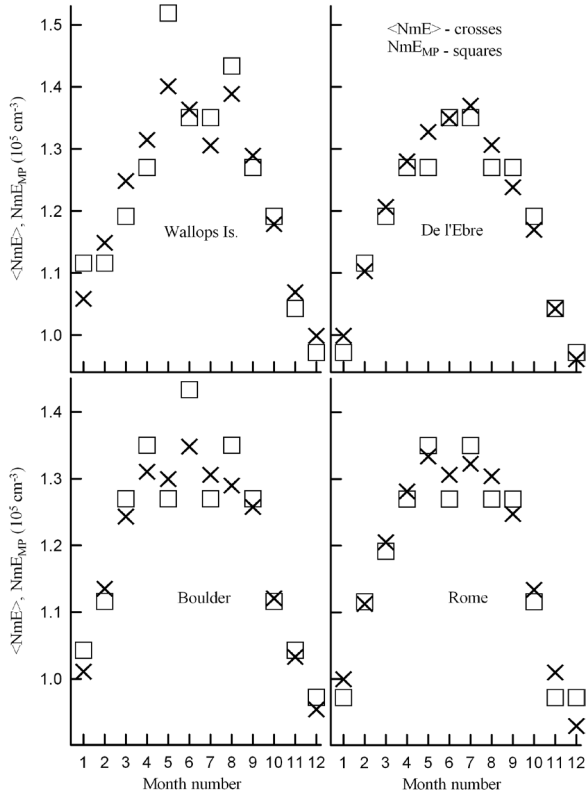
Figure 2. Month-to-month variations of the mathematically expected NmE (crosses) and the most probable NmE (squares) over the Wallops Island (left top panel), Boulder (left bottom panel), de l'Ebre (right top panel), and Rome (right bottom panel) ionosondes.

Figure 3. Month-to-month variations of the standard deviations of NmE from <NmE> (crosses) and from NmE_{MP} (squares) over the Wallops Island (left top panel), Boulder (left bottom panel), de l'Ebre (right top panel), and Rome (right bottom panel) ionosondes.

des are considered then the value of CV_{AV} is located in the range of 5.1-11.9 %. We point out that the calculated coefficients of variations of NmE relative to <NmE> presented in Figure 4 (6.7-10.6 % in March and 6.0-7.7 % in October) are comparable with that given by *Moore et al.* [2006].

The primary source of metals existing in the mesosphere and low thermosphere as metallic layers [e.g., Na, Fe, Ca, Mg, and K] is ablation of meteoroids in the atmosphere [see, e.g., *Kopp*, 1997; *Ceplecha et al.*, 1998; *Plane et al.*, 2015, and references therein]. After ablation, metal vapor densities are changed by diffusion and chemical reactions of metals with components of the atmosphere, forming altitude distributions of metal atoms at altitudes of the ionosphere. In addition to the ionization of metal atoms in their hyperthermal collisions with N_2, O_2, and O, chemical reactions of these metals with O_2^+ and NO^+ ionospheric ions produce metal ions at E- and D-region altitudes of the ionosphere [see, e.g., *Pavlov*, 2014, and references therein]. A sharp change in the direction of the hydrodynamic velocity of the atmosphere (wind shift) causes changes in number densities of metallic ions, forming a thin long-lived sporadic Es-layer electron number density at middle latitudes,
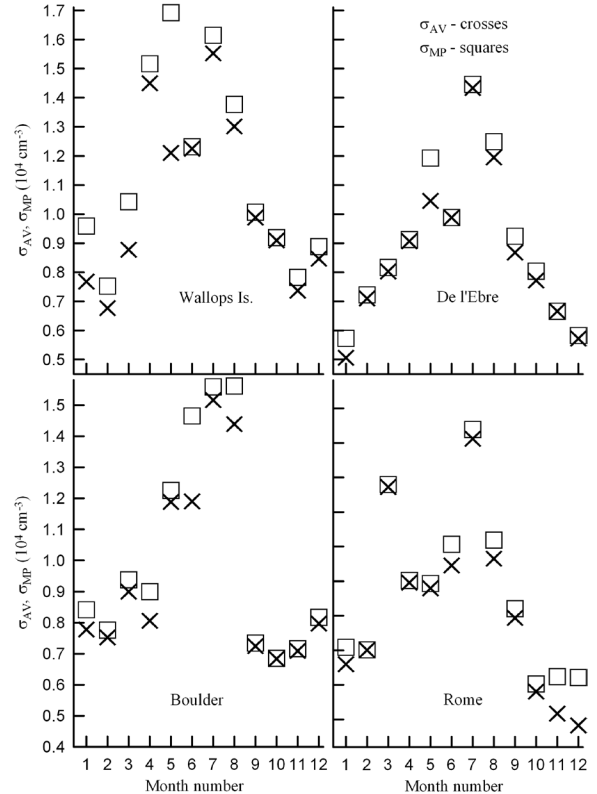
and the presence of slowly recombining metallic ions is responsible for these Es-layers having the properties of their irregular appearance in time and space [see, e.g., *Whitehead*, 1989; *Haldoupis*, 2012, and references therein]. As a result of the ablation of meteoroids, metallic ions exist not only in the Es-layer, but also at all E-region altitudes of the ionosphere above and below this Es-layer, and number densities of metallic ions under consideration are changed in time and in space. Furthermore, a par of metallic ions is transported along magnetic field lines by diffusion and plasma drift, and metallic ions are observed even at F-region altitudes of the ionosphere [e.g., *Fesen and Hays*, 1982; *McNeil et al.*, 1996; *Carter and Forbes*, 1999; *Collins et al.*, 2002; and references therein]. Thus, it can be assumed that a part of σ_{AV} and a part of CV_{AV} are produced by variations of metallic ion number densities.

The meteoroid influx into the atmosphere consists of showers when the Earth passes through meteoroid streams and sporadic meteoroids that do not belong to any specific meteoroid stream. The showers are divided into the major and minor meteor showers, and basic parameters of major meteor showers (period of activity, maximum date and so-
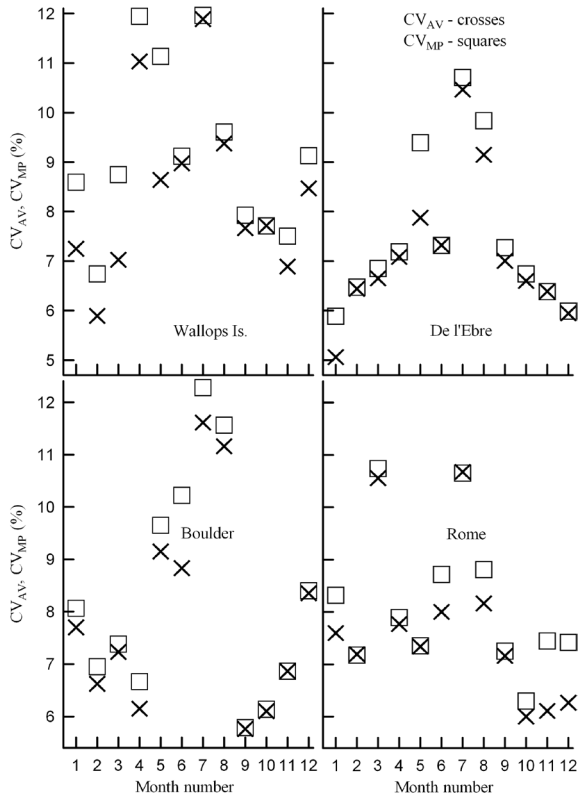
Figure 4. Month-to-month variations of the NmE variation coefficients relative to <NmE> (crosses) and NmE_{MP} (squares) over the Wallops Island (left top panel), Boulder (left bottom panel), de l'Ebre (right top panel), and Rome (right bottom panel) ionosondes.

lar longitude, duration defined as the width of the rate profile at one-quarter of the maximum, radiant, approximate local time of the radiant transit, geocentric velocity and orbital elements) are presented in Table XXII given by *Ceplecha et al.* [1998]. Some showers have a not regular annual activity, sometimes low, sometimes high, and changes in structures of meteoroid streams result in occasional intense outbursts or enhancements in their activity [*Ceplecha et al.*, 1998]. As a result, month-to-month changes of basic parameters of major meteor showers may have an impact on a part of month-to-month variations of σ_{AV} and CV_{AV} shown in Figs. 3 and 4, respectively. In particular, the absence of major meteor showers in February, March, June, and August [see Table XXII given by *Ceplecha et al.*, 1998] should manifest itself in the calculated values of σ_{AV} and CV_{AV}.

It follows from the calculations that the value of σ_{AV} and CV_{AV} is changed from one ionosonde to other ionosonde at given month of a year (see Figs. 3 and 4). We believe that these variations of σ_{AV} or CV_{AV} are caused by changes of <NmE> from one ionosonde to other ionosonde and by differences in meteoroid populations for locations of the meteoroid influx into the atmosphere at the locations of

the ionosondes (i.e., due to irregular distributions of metallic ion clouds in latitude and longitude).

4. Conclusions

The long-term statistical analysis of the month-to-month variations of mid-latitude noon NmE measured by the Wallops Island, Boulder, de l'Ebre, and Rome ionosondes during quiet times in 1957-2014 revealed notable contributions to the commonly accepted morphology of these variations.

The probability of the occurrence of a geomagnetically quiet NmE measured by each from 4 mid-latitude ionosondes was calculated at UT close to noon for each month in a year. We found that there are at list two peaks in each dependence of this probability on NmE, and, as a rule, the amplitude of the second-large peak is not much less than amplitude of the greatest peak that determines the most probable NmE. We provide evidence that the calculated month-to-month variations of the most probable NmE are the less efficient estimation of month-to-month variations of NmE in comparison with the expectation, <NmE>, of NmE.

The annual maximum of <NmE> is formed in May (Wallops Island and Rome), June (Boulder), and July (de l'Ebre), and the value of <NmE> is lowest in its annual value in December. A ratio of the largest to lowest value of <NmE> that characterizes the maximal month-to-month variability of <NmE> in a year is found to be in the range of 1.40-1.43. We report evidence that there is no the <NmE> winter anomaly.

The standard deviation of NmE from the mathematically expected NmE and the coefficient of variations of NmE relative to <NmE> calculated in this paper allow to quantitatively describe day-to-day variability of mid-latitude noon NmE during each month in a year at low solar activity. We found that the standard deviation of NmE from <NmE> maximizes in its annual value in July, while the lowest annual value of this statistical parameter of NmE is found to be in January (de l'Ebre), February (Wallops Island), October (Boulder), and December (Rome). The annual maximum of the coefficient of variations of NmE relative to <NmE> occurs in July over the ionosondes under consideration. This statistical parameter of NmE is minimal in January, February, September, and October over the de l'Ebre, Wallops Island, Boulder, and Rome ionosondes, respectively. The calculated value of this coefficient of variations of NmE is in the range of 5.1-11.9 %.

References

Akasofu, S.I., and S. Chapman (1972). Solar-terrestrial physics, Clarendon Press, Oxford.

Acebal, A.O., and J.J. Sojka (2011), A flare sensitive 3 h solar flux radio index for space weather applications, Space Weather, 9, S07004, doi:10.1029/2010SW000585.

Banks, P.M., and G. Kockarts (1973). Aeronomy. Part B, Academic Press, New York and London.

Carter, L.N., and J.M. Forbes (1999). Global transport and localized layering of metallic ions in the upper atmosphere, Ann. Geophysicae, 17, 190–209.

Ceplecha, Z., J. Borovička, W.G. Elford, D.O. Revelle, R.L. Hawkes and V.Š.M.

Porubčan (1998). Meteor Phenomena and Bodies, Space Sci. Rev., 84, 327-471.

Collins, S.C., J.M.C. Plane, M.C. Kelley, T.G. Wright, P. Soldán, T.J. Kane, A.J. Gerrard,

B.W. Grime, R.J. Rollason, J.S. Friedman, S.A. Gonzalez, Q. Zhou, M.P. Sulzer and C.A. Tepley (2002). A study of the role of ion-molecule chemistry in the formation of sporadic sodium layers, J. Atmos. Sol. - Terr. Phys., 64, 845-860.

Fesen, C.G., and P.B. Hays (1982). Mg^+ morphology from visual airglow experiment observations, J. Geophys. Res., 87, 9217-9223.

Haldoupis, C. (2012). Midlatitude Sporadic E. A Typical Paradigm of Atmosphere-Ionosphere Coupling, Space Sci. Rev., 168, 441-461.

Hedin, A.E. (1987). MSIS-86 thermospheric model, J. Geophys. Res., 92, 4649-4662.

Johnson, N.L. and F.C. Leone (1977). Statistics and experimental design in engineering and the physical Sciences, Vol. I., Second edition, John Wiley & Sons, New York - London - Sydney – Toronto.

Kouris, S.S., and D.N. Fotiadis (2002). Ionospheric variability: a comparative statistical study, Adv. Space Res., 29(6), 977-985.

Kopp, E. (1997). On the abundance of metal ions in the lower ionosphere, J. Geophys. Res., 102, 9667–9674.

Manson, J.E. (1976). The solar extreme ultraviolet between 30 and 205 A on November 9, 1971, compared with previous measurements in this spectral region, J. Geophys. Res., 81, 1629–1635.

McNeil, W.J., R.A. Dressler and E. Murad (2001). Impact of a major meteor storm on Earth's ionosphere: a modeling study, J. Geophys. Res., 106, 10447-10466.

Moore, L., M. Mendillo, C. Martinis and S. Bailey (2006). Day-to-day variability of the E layer, J. Geophys. Res., 111, A06307, doi:10.1029/2005JA011448.

Nicolls, M.J., F.S. Rodrigues and G.S. Bust (2012). Global observations of E region plasma density morphology and variability, J. Geophys. Res., 117, A01305, doi:10.1029/2011JA017069.

Pavlov, A.V. (2012). Ion Chemistry of the Ionosphere at the E- and F-region Altitudes: A Review, Surveys in Geophysics, 33, 1133-1172.

Pavlov, A.V., and N. M. Pavlova (2005). Causes of the mid-latitude NmF2 winter anomaly, J. Atmos. Sol. Terr. Phys., 67, 862–877.

Pavlov A.V., and N.M. Pavlova (2009) Anomalous variations of NmF2 over the Argentine Islands: a statistical study, Ann. Geophysicae, 27, 1363–1375.

Pavlov, A.V., N. M. Pavlova, and S. F. Makarenko (2010). A statistical study of the mid-latitude NmF2 winter anomaly, Adv. Space Res., 45(3), 374–385.

Pavlov, A.V., and N.M. Pavlova (2013). Comparison of NmE measured by the Boulder ionosonde with model predictions near the spring equinox, J. Atmosph. Solar-Terr. Phys., 102, 39–47.

Pavlov, A.V., and N.M. Pavlova (2014). Influence of the equinoctial asymmetry on the semi-annual anomaly in NmF2 near noon in the northern geographic hemisphere: a statistical study, Adv. Space Res., 53(4), 619-634.

Pavlov, A.V., and N.M. Pavlova (2015). Comparison of Electron Concentrations in the Ionospheric E-Layer Maximum in Spring Conditions Obtained by Calculations and Moscow Ionosonde Measurements, Geomagnetism and Aeronomy, 55, 235–245, doi:10.1134/S0016793215040118.

Picone, J.M., A.E. Hedin, D.P. Drob, and A.C. Aikin (2002). NRLMSISE-00 empirical model of the atmosphere: statistical comparisons and scientific issues, J. Geophys. Res., 107, 1468, doi:10.1029/2002JA009430.

Piggott, W. R. and K. Rawer (Eds.) (1978). URSI handbook of ionogram interpretation and reduction, National Oceanic and Atmospheric Administration, CO, Boulder.

Plane, J.M.C., W. Feng and E.C.M. Dawkins (2015). The Mesosphere and Metals: Chemistry and Changes, Chemical Reviews, 115, 4497–4541.

Richards, P.G., J.A. Fennelly and D.G. Torr (1994). EUVAC: A solar EUV flux model for aeronomical Calculations, J. Geophys. Res., 99, 8981-8992.

Schunk, R.W., and A.F. Nagy (2009). Ionospheres.

Physics, plasma physics, and chemistry. University Press, Cambridge.

Sojka, J.J., J.B. Jensen, M. David, R.W. Schunk, T. Woods, F. Eparvier, M.P. Sulzer,

S.A. Gonzalez, and J.V. Eccles (2014) Ionospheric model-observation comparisons: E layer at Arecibo Incorporation of SDO-EVE solar irradiances, J. Geophys. Res., 119, 3844−3856.

Solomon, S.C. (2006). Numerical models of the E-region ionosphere, Adv. Space Res., 37 (5),1031–1037.

Whitehead, J.D. (1989). Recent work on mid-latitude and equatorial sporadic-E, J. Atmos. Terr. Phys., 51, 401–424.

---

*Corresponding author: Anatoli Pavlov, Pushkov Institute of Terrestrial Magnetism, Ionosphere and Radio Wave Propagation (IZMIRAN), Russia Academy of Science,142190, Troitsk, Moscow, Russia; e-mail: pavlov@izmiran.ru